IEEE Access
Multidisciplinary | Rapid Review | Open Access Journal

Received March 29, 2021, accepted April 15, 2021, date of publication April 26, 2021, date of current version May 4, 2021.

*Digital Object Identifier 10.1109/ACCESS.2021.3075906*

# Development of an Experimental Scaled-Down Frequency Dependent Transmission Line Model

**KIRAN KUMAR CHALLA, (Member, IEEE), AND GURUNATH GURRALA, (Senior Member, IEEE)**
Indian Institute of Science, Bengaluru 560012, India

Corresponding author: Kiran Kumar Challa (kiranc@iisc.ac.in)

This work was supported by the Fund for Improvement of Science and Technology (FIST) program, Department of Science and Technology (DST), India, through the project "Smart Energy Systems Infrastructure Hybrid Test Bed" under Grant SR/FST/ETII-063/2015 (C) and (G).

**ABSTRACT** The penetration of power electronic based equipment in the power grid has increased the co-occurrence of electromechanical and electromagnetic transients. Significant research efforts have been focused in the last decade to study these interactions. Frequency dependent transmission line models are indispensable to understand such interactions. This paper describes a systematic procedure for the development of an experimental scaled-down 220 V frequency dependent transmission line model of a 230 kV transmission line. A reduced order lumped parameter frequency dependent transmission line using modal transformation is derived for the 230 kV transmission line and scaled-down to 220 V. Clarke and inverse Clarke transformations are implemented using specially designed 1-$\phi$ transformers. The inductances of the scaled-down model are realized using amorphous cores. Line energization, balanced, and unbalanced fault studies are carried out using the experimental line. The experimental results are compared with the simulation results of a universal line and a constant parameter $\pi$-model using EMTP-RV. The proposed experimental line properly captured important features of the frequency dependent line such as smoother wave shape during energization, traveling time, currents, and voltage magnitudes during the fault and after the fault removal.

**INDEX TERMS** Amorphous core inductors, frequency dependent transmission line models, lumped parameter models, modal transformation matrix, switching transients, unbalanced faults, universal line model.

## I. INTRODUCTION

The synchronous generator dominated power systems have been gradually transforming into the converter dominant power grids with high penetration of renewable energy sources, HVDC transmission and FACTS devices. The presence of power electronic converters increases the co-occurrence of electromechanical and electromagnetic transients to a great extent [1]. The narrowed difference in occurrence between these two types of transients necessitates detailed modeling of individual components in power system. Availability of detailed models and the advancement in real-time simulators have completely replaced the experimental models of electric power systems across the world [2]–[6].

In spite of having several technical and economic advantages for the digital simulators, physical laboratory models of power systems components continued to be the important part of power system research. The physical laboratory models are miniature reproduction of actual power systems and they are cheaper for the proof of concept on small test systems such as single machine infinite bus (SMIB), 3 or 4 mchine systems [7]–[9]. Transmission line is the most important part in the physical model of SMIB. Lumped parameter transmission lines are quite often used in power systems simulation studies [10]–[13]. A methodology is presented in [10], [11] to consider the non-transposed and frequency dependent parameters in designing transmission line models. Analysis of the number of cascaded $\pi$ or T sections required for the accurate representation of line according to the frequency range of interest is presented in [12], [13]. There are several attempts in literature to develop experimental models of these lumped parameter lines for the power system studies. In [14]–[18], lumped parameter based models which represent the line as a constant parameter cascaded $\pi$-sections were used. Lumped parameter models introduce additional frequencies which are

The associate editor coordinating the review of this manuscript and approving it for publication was Siqi Bu.

not present in the system and may cause undesirable interactions [19]. In [20], a scaled-down lumped transmission line including mutual coupling between the phases and neutral is developed. In [21]–[23], the transmission lines are emulated using power electronic converters. The line is emulated as a series resistance and inductance in [22], as cascaded $\pi$-sections in [21] and as a Bergeron distributed parameter model in [23]. Emulation of frequency dependent lines using power electronic converters require high bandwidth converters, high sampling rate data acquisition and high computational power for the controllers [23]. Frequency dependency of transmission line parameters is important in correctly reproducing the transient responses due to the interactions. This is more pronounced when the zero sequence modes are involved during unbalanced fault conditions as well as in the case of harmonic load flow analysis [24].

Notable research went into the development of the frequency dependent (FD) transmission line models for digital computer simulations [25]–[37]. But, there are no efforts in literature on the development of a scaled-down experimental model of frequency dependent transmission line to the best of our knowledge. This paper is an attempt in that direction. The widely used universal line model (ULM) [30] and Marti's model [29] requires realization of dependent voltage or current sources. Hence, in this paper an attempt is made to physically realize a lumped parameter frequency dependent (LPFD) model proposed in [36]. Modal domain LPFD line using the Clarke's transformation matrix was proposed by in [38], [39]. In [38], [39], the modal transformations (Clarke and inverse Clarke transforms) are represented using single phase ideal transformers [40] and each mode of the line is represented through a cascade connection of $\pi$-circuits. Frequency dependence of longitudinal parameters in $\pi$-circuits was incorporated though synthesized circuits consisting of series and parallel resistors and inductors, with each $\pi$-circuit representing 10 $km$ length [39]. Performance of this modal domain lumped parameter frequency dependent (LPFD) line is compared in [41] with the other frequency dependent transmission line models proposed in [27]–[29]. Comparison presented in [41] concludes that, even though the LPFD line has some simplifications, it produces more accurate results comparable to the other models. LPFD line is further applied to double three phase transmission lines in [42] and validated for three types of line transpositions and non transposed lines. State space representation of LPFD line is presented in [36] to evaluate transients in lines.

For the physical realization of scaled-down model of LPFD line, a scale-down procedure to convert the 230 $kV$ lines to a 220 $V$ laboratory voltage level is proposed in [43]. In [43], standard tower and conductor configurations of 230 $kV$ lines are selected to match the per unit impedances of the WECC 3-machine 9-bus system and then LPFD model proposed in [36] are obtained. In this paper, the LPFD line between buses 7 and 8 in the WECC system is physically realized. The transformation matrices (Clarke and inverse Clarke transforms) in this paper are physically realized using specially designed single phase transformers. The inductances of the passive equivalent circuit are realized using amorphous core inductors to achieve constant inductance over a wide frequency range. This helps in faith full reproduction of the switching transients in the LPFD line. The procedure used for the design of amorphous core inductors is described. Line energization, balanced and unbalanced fault studies are carried out on the developed 50 $km$ experimental LPFD line. The experimental results are compared with the simulation results of a universal line model (ULM) and a constant parameter $\pi$-model using EMTP-RV.

## II. LUMPED PARAMETER FREQUENCY DEPENDENT TRANSMISSION LINE MODEL (LPFD)

Depending on the accuracy requirements and the application, transmission line models are mainly classified into two types as constant parameter lines and frequency dependent lines. For analyzing the transients over a wide frequency spectrum, a frequency dependent distributed parameter line should be considered. Among the all available FD line models, universal line model (ULM) [30] and Marti's model [29] are widely used in all the commercial electromagnetic transient programs. But, physical implementation of these model requires physical realization of dependent voltage or current sources. In [36], a lumped parameter based frequency dependent (LPFD) transmission line is proposed. An $n$-phase line is represented in the modal domain by decomposing the '$n$' phase line into '$n$' exact modes in which each mode can be considered as a single phase line [36].

### A. MATHEMATICAL MODEL OF LPFD LINE

Mathematical formulation of the lumped parameter frequency dependent model of a transmission line shown in Fig.1 with per unit length parameters is given by,

$$-\frac{dV(x,\omega)}{dx} = Z(\omega)I(x,\omega) \tag{1}$$

$$-\frac{dI(x,\omega)}{dx} = Y(\omega)V(x,\omega) \tag{2}$$

where:

$V(x,\omega)$: Line voltage at coordinate $x$

$I(x,\omega)$: Line current at coordinate $x$

$Z(\omega) = R(\omega) + j\omega L$: Series impedance per unit length

$Y(\omega) = G + j\omega C$: Shunt admittance per unit length

Differentiating (1) and (2), one can get the voltage and current propagation equations for the line,

$$\frac{d^2V(\omega)}{dx^2} = Z(\omega)Y(\omega)V(\omega) \tag{3}$$

$$\frac{d^2I(\omega)}{dx^2} = Y(\omega)Z(\omega)I(\omega) \tag{4}$$

In order to transform the phase quantities to a modal domain, either a transformation matrix is obtained from the frequency dependent impedance $Z(\omega)$ and admittance $Y(\omega)$ matrices of the transmission line or Clarke's transformation

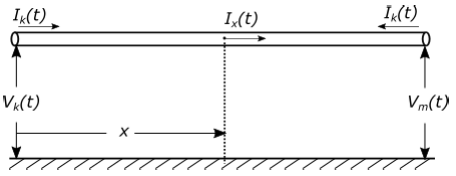


**FIGURE 1.** Frequency dependent transmission line.

matrix given in (5) with constant and real elements is used [44], [45]. As the Clarke's transformation is real and constant, it is used in the development of physical model. This transformation gives an exact solution for transposed line and a good approximation for non-transposed lines with a vertical symmetry plane [45]. Similarly, $V(\omega)$ and $I(\omega)$ are converted from phase domain to modal domain using (5).

$$T_{clk} = \begin{bmatrix} \frac{2}{\sqrt{6}} & 0 & \frac{1}{\sqrt{3}} \\ \frac{-1}{\sqrt{6}} & \frac{1}{\sqrt{2}} & \frac{1}{\sqrt{3}} \\ \frac{-1}{\sqrt{6}} & \frac{-1}{\sqrt{2}} & \frac{1}{\sqrt{3}} \end{bmatrix} \tag{5}$$

Inverse modal transformation matrix ($T_{clk}^{-1}$) is give by,

$$T_{clk}^{-1} = \begin{bmatrix} \frac{2}{\sqrt{6}} & \frac{-1}{\sqrt{6}} & \frac{-1}{\sqrt{6}} \\ 0 & \frac{1}{\sqrt{2}} & \frac{-1}{\sqrt{2}} \\ \frac{1}{\sqrt{3}} & \frac{1}{\sqrt{3}} & \frac{1}{\sqrt{3}} \end{bmatrix} \tag{6}$$

After transforming the line equations from the phase domain to the modal domain, the transmission line is represented by the following equations,

$$\frac{d^2 I_m(\omega)}{dx^2} = Y_m(\omega) Z_m(\omega) I_m(\omega) \tag{7}$$

$$\frac{d^2 V_m(\omega)}{dx^2} = Z_m(\omega) Y_m(\omega) V_m(\omega) \tag{8}$$

In (7) and (8), the vectors $V_m(\omega)$ and $I_m(\omega)$ are transversal voltages and longitudinal currents in modal domain. Matrices $Z_m(\omega)$ and $Y_m(\omega)$ are per unit length longitudinal impedance and shunt admittance matrices respectively. The relationship between phase and modal quantities is given as follows,

$$Z_m = T_{clk}^t Z T_{clk} = \begin{bmatrix} Z_\alpha & 0 & Z_{\alpha 0} \\ 0 & Z_\beta & 0 \\ Z_{\alpha 0} & 0 & Z_0 \end{bmatrix} \tag{9}$$

$$Y_m = T_{clk}^{-1} Y (T_{clk}^{-1})^t = \begin{bmatrix} Y_\alpha & 0 & Y_{\alpha 0} \\ 0 & Y_\beta & 0 \\ Y_{\alpha 0} & 0 & Y_0 \end{bmatrix} \tag{10}$$

$$V_m = T_{clk}^t V \quad I_m = T_{clk}^{-1} I \tag{11}$$

The non zero off-diagonal elements become insignificant when compared to the diagonal elements depending on the line characteristics [46]. Therefore, mutual terms $Z_{\alpha 0}$ and $Y_{\alpha 0}$ are discarded in (9) and (10). Then all the modes are declared as exact modes and transmission line representation in modal domain is obtained as shown in Fig.2. Each mode is then represented by a cascaded connection of multiple $\pi$-circuits as shown in Fig.2 where $Z_{ms}$ represents the corresponding modal impedance ($Z_\alpha$ or $Z_\beta$ or $Z_0$).

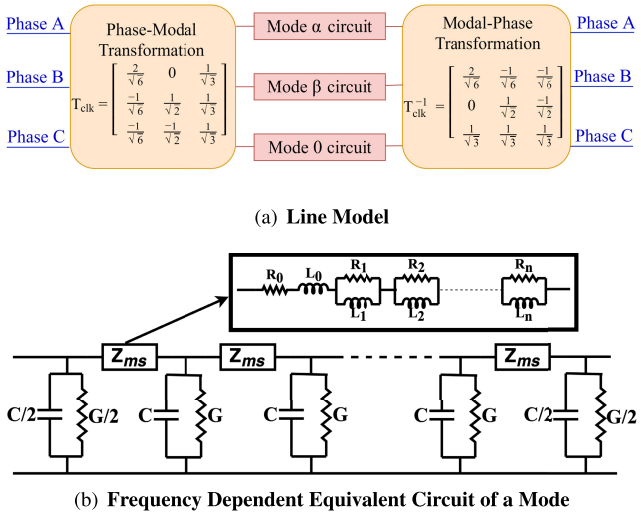


(a) **Line Model**

(b) **Frequency Dependent Equivalent Circuit of a Mode**

**FIGURE 2.** LPFD transmission line model.

### B. LINE SELECTION & LPFD MODEL

In [43], frequency dependent lines for the WECC system are obtained by properly choosing the tower and conductor configurations close to the practical towers [47] so that the *per-km* impedances and the steady state power flows are matched as much as possible to the original system. From these lines of WECC 3-machine 9-bus system, a un-transposed line between buses 7 and 8 is chosen for physical realization in this paper. Tower and conductor configuration of the selected line are shown in Table.1. The modal impedance and admittance of the line are obtained using (9) and (10) for a frequency range of 1 mHz to 100 MHz with 10 points/decade. Mutual terms in these matrices are neglected since they are insignificant [36].

Foster R-L equivalents are fitted to the frequency response of the individual modal impedances using the algorithm proposed by the authors in [37], [48]. The algorithm is based on the positive peaks, negative peaks and positive zero crossings of change in slope ($\Delta$Slope) of the modal impedances and it reduces the number of passive elements in LPFD model. According to the proposed algorithm, Positive and negative peaks of $\Delta$Slope indicates the number of zeros and poles required for fitting.

The frequency response of each mode impedance and the corresponding fitted R-L equivalent circuit responses are shown in Fig.3. From Fig.3, it can be observed that the $\Delta$Slope of *Mode-*$\alpha$ and *Mode-*$\beta$ have one positive peak (i.e. no positive zero crossing) and no negative peaks. This indicates that these modal impedances have a single zero and

**TABLE 1.** Tower and conductor data 230kV line [43].

| Phase No | DC resistance [Ω/km] | Outer diameter [cm] | Horizontal distance [m] | Vertical Height at tower [m] | Vertical Height at midspan [m] |
|---|---|---|---|---|---|
| 1 | 0.0856 | 2.524 | -9 | 16.74 | 13.394 |
| 2 | 0.0856 | 2.524 | 0 | 16.74 | 13.394 |
| 3 | 0.0856 | 2.524 | 9 | 16.74 | 13.394 |
| 0 | 2.362 | 1.144 | -6.5 | 23.24 | 18.592 |
| 0 | 2.362 | 1.144 | 6.5 | 23.24 | 18.592 |

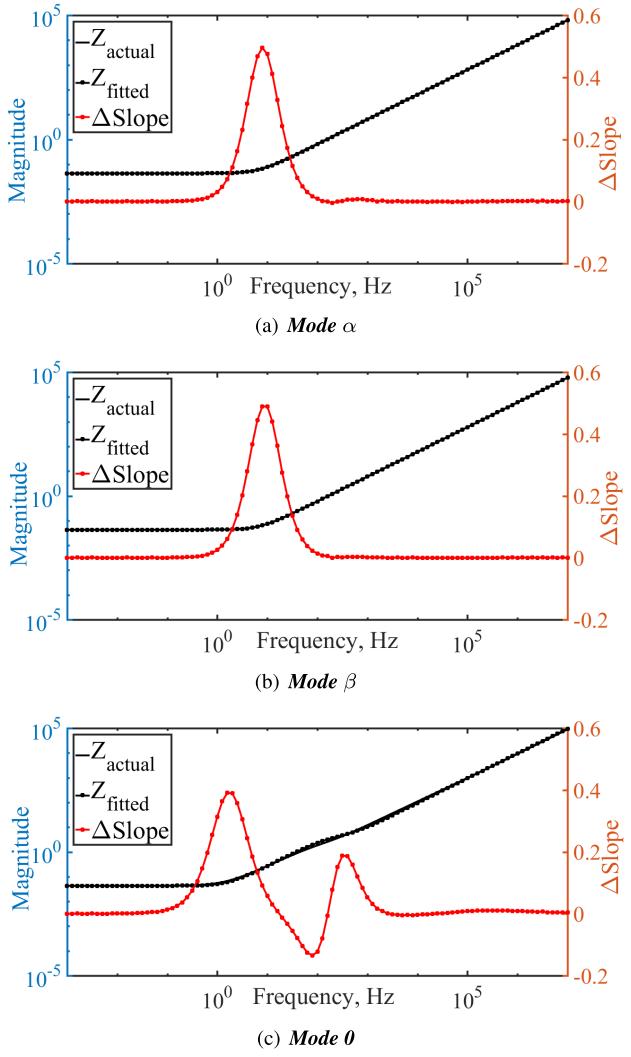


(a) ***Mode*** $\alpha$

(b) ***Mode*** $\beta$

(c) ***Mode 0***

**FIGURE 3.** Frequency response of model and fitted impedances.

no poles. So, a single series $R_0, L_0$ branch is sufficient to fit these modal responses. Also, one can observe the presence of two positive peaks (one positive zero crossing) and one negative peak in $\Delta Slope$ of *Mode-0* responses in Fig.3(c). This indicates that the *Mode-0* impedance has two zeros and one pole. So, a first order system having two zeros ($G_0(s)$ and $G_1(s)$) with $R_0, R_1, L_0$ and $L_1$ is fitted to the *Mode-0* impedance of all the lines. Elements of the 230 kV LPFD model are scaled-down to a 220 V laboratory voltage level using the following expression [43],

$$Z^{sd}_{actual} = Z_{actual} \times \frac{S^{old}_{base}}{{V^{old}_{base}}^2} \times \frac{S^{sd}_{base}}{{V^{sd}_{base}}^2} \tag{12}$$

where $Z^{sd}_{actual}$ = actual value of impedance in scaled-down system, $Z_{actual}$ = actual value of impedance in original system, $S^{old}_{base} = 247.5$ MVA, $V^{old}_{base} = 230$ kV, $S^{sd}_{base} = 5$ kVA and $V^{sd}_{base} = 220$ V.

In [19], propagation velocity, attenuation factor and surge impedance of $\pi$-section equivalent circuit are compared with the distributed parameter circuit to find out the number of necessary sections (length of each $\pi$-section) for accurately representing the transmission line for transient analysis. Equivalent length of each $\pi$-section is identified to be 10 *km* in [19]. The accuracy of line is verified with different $\pi$-section lengths varied from 2.5 km to 10 km. Voltage transients for the line energization and fault removal for different $\pi$-section lengths in comparison with universal line model are presented in Figure.4. It is evident from Figure.4 that the 10 km length of $\pi$-section is adequate and gives similar results as the 2.5 km length. So, the length of 10 *km* for $\pi$-section is used in the experimental line. For a 10km section, resistance, inductance, capacitance and conductance of the modal equivalent circuit of the proposed scaled-down LPFD line are given in the Table.2. To realize a 50km line, 5-sections are used in simulations and experimental validation.

**TABLE 2.** Elements of scaled-down LPFD line for a 10km section.

| **Element** | **Mode 0** | **Mode** $\alpha$ | **Mode** $\beta$ |
|---|---|---|---|
| **Lo** (mH) | 1.2124 | 0.4755 | 0.4302 |
| **L1** (mH) | 0.8981 | - | - |
| **Ro** (Ω) | 0.0194 | 0.0194 | 0.0194 |
| **R1** (Ω) | 0.4128 | - | - |
| **C** (nF) | 1753.2 | 2420 | 2676.2 |
| **1/G** (MΩ) | 90.579 | 90.579 | 90.579 |

## III. PHYSICAL REALIZATION OF LPFD MODEL

Two important things to be addressed in the physical realization of LPFD model are

1) Physical realization of the Clarke's transform and it's inverse.
2) The design of high frequency inductors.

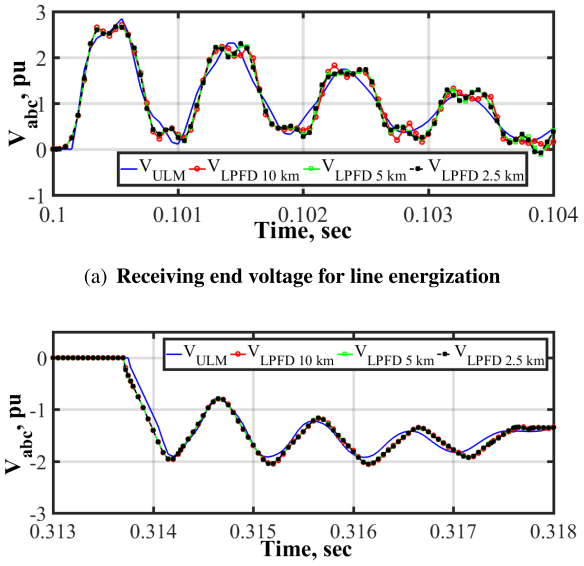


(a) **Receiving end voltage for line energization**

(b) **Receiving end voltage after fault removal**

**FIGURE 4.** **Transient response of the receiving end voltage for different $\pi$ section lengths.**

### *A. PHYSICAL IMPLEMENTATION OF THE CLARKE's AND INVERSE CLARKE's TRANSFORMS*

Clarke's transformation matrix is practically realized using multiple 1-$\phi$ transformers. The modal voltages, $V_\alpha, V_\beta, V_0$ and the modal currents $I_\alpha, I_\beta, I_0$ are obtained using the transformation as follows:

$$T_{clk}^T = \begin{bmatrix} \frac{2}{\sqrt{6}} & \frac{-1}{\sqrt{6}} & \frac{-1}{\sqrt{6}} \\ 0 & \frac{1}{\sqrt{2}} & \frac{-1}{\sqrt{2}} \\ \frac{1}{\sqrt{3}} & \frac{1}{\sqrt{3}} & \frac{1}{\sqrt{3}} \end{bmatrix} \tag{13}$$

$$V_{\alpha\beta 0} = T_{clk}^T V_{abc} \tag{14}$$

$$I_{\alpha\beta 0} = T_{clk}^T I_{abc} \tag{15}$$

The secondary voltage rating and turns ratio of each 1-$\phi$ transformer are decided according to the elements in the Clarke's transformation. For example, three single phase transformers connected to $V_{an}$, $-V_{bn}$ and $-V_{cn}$ with turns ratios, $\sqrt{6}:2$, $\sqrt{6}:1$ and $\sqrt{6}:1$ respectively are used for $Mode-\alpha$. Secondary terminals of these three transformers are connected in series (maintaining proper sign convention) to get the *Mode* $\alpha$ voltage. Similarly, *Mode*-$\beta$ and *Mode*-0 voltages are derived using two and three 1-$\phi$ transformers respectively with appropriate turns ratios. The proposed implementation is shown in Fig.5.

Current ratings of the transformer windings are selected as the maximum possible currents through each mode during all possible loading conditions. $Mode-\alpha$ and $Mode-\beta$ currents will attain a maximum value of $\sqrt{\frac{3}{2}} \times I_a$ under 3-$\phi$ balanced loading conditions. So, these currents are calculated for a balanced load of 3-$\phi$, 5 kVA, 220 V at the far end of the

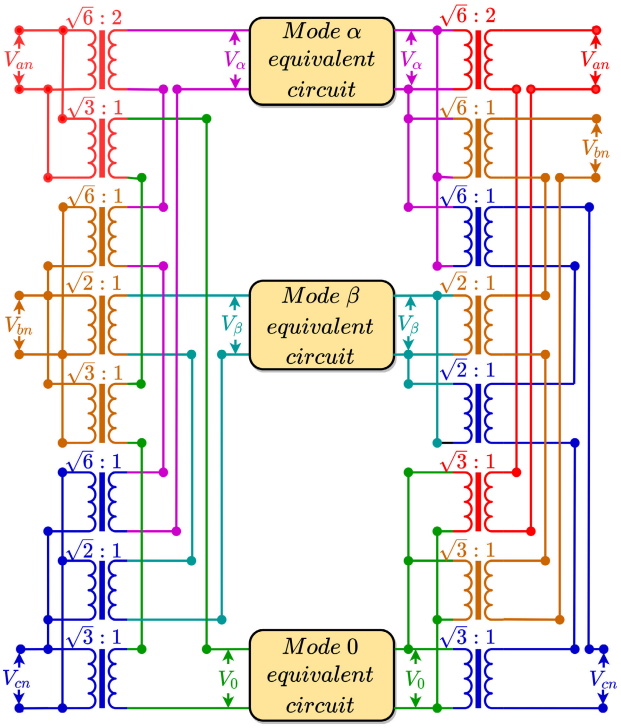


**FIGURE 5.** **Proposed LPFD line implementation.**

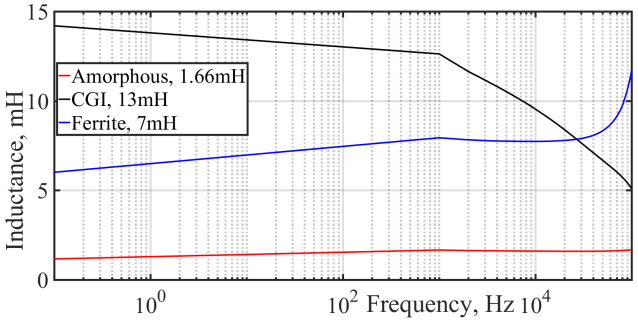


**FIGURE 6.** **Frequency response of different core inductors.**

transmission line as 16.07 A. The magnitude of $Mode-0$ current is zero for a balanced load and remains constant at $\frac{I_a}{\sqrt{(3)}}$ for 1-$\phi$ or 2-$\phi$ loading. So, $Mode-0$ maximum current is calculated as 7.575 A for a 1-$\phi$, 1.66 kVA load connected to any one of the phases. Similar procedure is followed to realize the inverse transformation matrix.

VA rating of the transformers in the modal transformation is calculated as the product of the secondary voltage rating and the maximum possible current through the corresponding mode. The calculated ratings of all the 1-$\phi$ transformers are given in Table.3. All the transformers are specially designed (through a local vendor) to reduce the leakage reactance as much as possible and carry 10 times the rated current for 2 s duration to withstand transient short circuit currents.

**TABLE 3.** Transformer ratings for the transformations.

| S.No | Turns ratio | Primary voltage [V] | Secondary voltage [V] | VA rating | Quantity required |
|---|---|---|---|---|---|
| Clarke's transformation | | | | | |
| 1 | $\sqrt{6}:2$ | 127 | 103.70 | 1666.66 | 1 |
| 2 | $\sqrt{3}:1$ | 127 | 73.32 | 630 | 3 |
| 3 | $\sqrt{6}:1$ | 127 | 51.84 | 840 | 2 |
| 4 | $\sqrt{2}:1$ | 127 | 89.80 | 1695 | 2 |
| Inverse Clarke's transformation | | | | | |
| 5 | $\sqrt{6}:2$ | 155.56 | 127.01 | 1666.66 | 1 |
| 6 | $\sqrt{3}:1$ | 155.56 | 89.81 | 570 | 3 |
| 7 | $\sqrt{6}:1$ | 155.56 | 63.50 | 833.22 | 2 |
| 8 | $\sqrt{2}:1$ | 155.56 | 108 | 1443.33 | 2 |

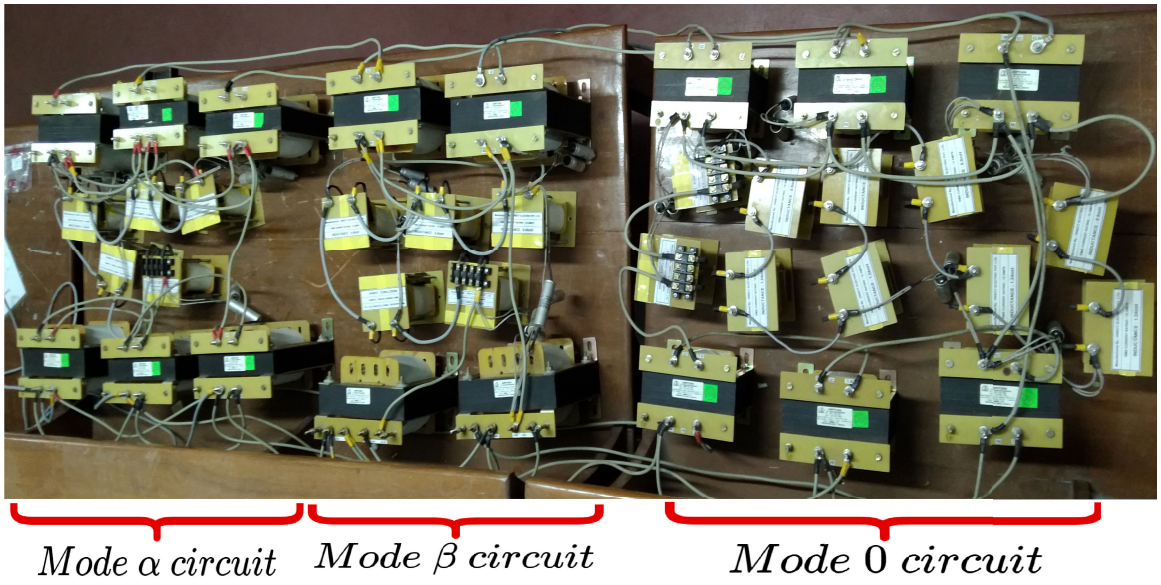


**FIGURE 7.** Experimental setup.

### *B. DESIGN PROCEDURE FOR HIGH FREQUENCY INDUCTORS*

The fitted inductors in the LPFD model should be designed to have constant inductance over a wide range of frequency in order properly to reproduce the switching transients (up to 5 kHz). The magnetic core should not saturate for the sub-transient currents ($\approx$ 10 times the rated current) during the short circuit conditions. Inductors of different core materials available in the laboratory are tested for their frequency dependency using a frequency response analyzer and the responses are presented in Fig.6. It is clear from these responses that the inductance of CGI core and ferrite core inductors change significantly after 500 Hz, whereas the amorphous core inductor has a constant inductance up to 50 kHz. Amorphous core inductors are also smaller in size, light weight and can handle higher flux densities when compared to the other core inductors. In this paper amorphous inductors are designed based on the area product approach [49]. The product of core cross-section area ($A_e$) and window area ($A_w$) in an inductor (area product) is a measure of the energy handling capability of the inductor. The area product ($A_p$) equation is a good starting point for the design since it relates the electrical design inputs with material and geometric constraints. Procedure for the design of inductors using the area product approach is given as follows [49],

- Calculate the area product required as per the specifications of the inductor.

$$A_p = A_e A_w = \frac{L I_{peak} I_{rms}}{k_u B_m J_m} \tag{16}$$

where, $L$ is the required inductance, $I_{peak}$ is the peak current rating of the inductor, $I_{rms}$ is the *rms* current rating of the inductor, $k_u$ is the window utilization factor, $B_m$ is the maximum flux density of the core material and $J_m$ is the current density of the conductor.
For example: $L = 450\ \mu$H, $I_{rms} = 17$ A, $I_{peak} = 170$ A, $k_u = 0.6$, $B_m = 1.4$ T, $J_m = 3$ A/$m^2$

$$A_p = A_e A_w = \frac{450 \times 170 \times 170}{0.6 \times 1.4 \times 3} = 5,16,071 \tag{17}$$

- Select a core with the area product greater than or equal to the requited area product and calculate the $A_e$ and $A_w$ for the selected core. For 450 $\mu$H inductor, AMCC 100 core is selected with $A_e = 590\ mm^2$, $A_w = 1400\ mm^2$ and $A_e \times A_w = 8,26,000$. Core with a higher area product is selected to make sure that the inductor doesn't saturate for sub-transient fault currents.
- Select an air gap from the $A_L$ curves published by the vendor [50]. For this $A_L$, calculate the number of turns $N$ required for the copper winding

$$N = \sqrt{\frac{L}{A_L}} \tag{18}$$

The unit of $A_L$ here is $\mu H/\ (turns)^2$. The air gap selected is more than the values specified in [50] to avoid the core saturation during the sub-transient short circuit currents. For 450 $\mu$H inductor, with air-gap of 8.2 $mm$ and $A_L$ of 0.05 $\mu H/\ (turns)^2$, number of turns required are calculated as 93.

- Calculate the peak flux density $B_m$ as

$$B_m = \frac{A_L N I_{peak}}{A_e} \tag{19}$$

If the core is saturated, increase the air gap and select new $A_L$. If it is not possible to choose a higher air gap, go to next larger core size. Peak flux density for 450 $\mu$H inductor is 1.34 T which is less than the peak flux density (1.4 T) of the selected amorphous core. This way one can ensure that the core does not saturate.

Design specifications of the inductors are given in the Table.4. It can be observed that the values selected are within the $\pm 10\%$ tolerance limits of the actual values. These values are selected in consultation with a local manufacturer.

**TABLE 4. Specifications of inductors.**

| Inductance ($\mu$H) | 900 | 1240 | 450 |
|---|---|---|---|
| RMS current (A) | 12 | 12 | 17 |
| Peak current (A) | 60 | 80 | 170 |
| Core | AMCC 50 | AMCC 100 | AMCC 100 |
| Peak flux density (T) | 1.4 | 1.4 | 1.4 |
| Current density ($A/m^2$) | 3 | 3 | 3 |
| Utilization factor ($k_u$) | 0.6 | 0.6 | 0.6 |
| Number of turns (N) | 118 | 121 | 93 |
| Air gap (mm) | 7.52 | 6.78 | 8.2 |
| Winding wire gauge | SWG 17 | SWG 17 | SWG 17 |
| No of parallel windings | 3 | 3 | 4 |

### C. DEVELOPMENT PROCEDURE FOR EXPERIMENTAL LPFD LINE

The procedure for building an experimental scaled-down lumped parameter frequency dependent transmission line for any voltage level is summarized as follows:

1) For a desired transmission line use its tower and conductor configurations in a EMTP line constants program to obtain the frequency response of the characteristic impedances. Then obtain the frequency responses of the modal impedances using (9) (see section II-A).
2) If only p.u. impedances of the lines are available then use the procedure explained in [43] to identify the tower and conductor configurations which will match the steady state performance i.e. the impedances and power flows of the selected line. Repeat step-1.
3) Derive the LPFD model inductances and capacitances from the frequency response curves of the model impedances using the algorithm presented in [48].
4) Scale-down the LPFD model to the desired laboratory voltage and power levels using (12).
5) Obtain ratings of the physical transformers needed for realization of the Clarke's and its inverse transformation as explained in Section III-A.
6) Design the high frequency inductors obtained in step-4 using the procedure discussed in section III-B. Try to keep the resistance of the inductors as low as possible. Also choose the capacitors (series/parallel combinations if required) to match the scaled down model capacitor values and ratings obtained in step-4. See Table.2 for the inductor and capacitor values used in this paper.
7) Develop the experimental LPFD line model by properly wiring the transformers, inductors and capacitors as per the equivalent circuit shown in Fig.5.

## IV. EXPERIMENTAL RESULTS

The developed scaled-down LPFD model of the 230 kV line using amorphous core inductors and the Clarke's transformation using 1-$\phi$ transformers is shown in Fig.7. In this model, the resistances of the equivalent circuit are not designed separately as the manufactured inductors resistance values are higher than the required resistance values. This line is referred as SD-LPFD line in this section.

### A. VALIDATION OF CLARKE's AND INVERSE CLARKE's IMPLEMENTATION

The effectiveness of the transformation matrix implementation using the transformers is tested using the laboratory mains voltages.

The SD-LPFD line 3-$\phi$ voltages/currents and the modal voltages/currents at the sending end constitute the input and output respectively for the developed Clarke's transformers. Fig.8 shows these voltages captured using an oscilloscope Similarly, the modal voltages/currents and the 3-$\phi$ voltages/currents at the receiving end constitute the input and output respectively for the developed inverse Clarke's transformers. Fig.9 shows these voltages measured using oscilloscope. It can be observed from Fig.8 that the CH1 voltage ($V_R$ - input to the transformation) and CH4 voltage ($V_\alpha$ - output of the transformation) are in phase with each other. In Fig.9, one can observe that the CH4 voltage ($V_\alpha$ - input to the inverse transformation) is in phase with the CH1 voltage ($V_R$ - output of the inverse transformation). Also

**TABLE 5.** Transformation implementation results.

| Clarke's Transformation | | | |
|---|---|---|---|
| Input $V_a, V_b, V_c$ | Output $V_\alpha, V_\beta, V_0$ | | |
| | Theoretical | Practical | Error (V) |
| 129.204∠0 | 158.22∠0.0 | 156.53∠0 | 1.69 |
| 129.133∠120.34 | 157.8321∠90.34 | 157.012∠90.052 | 1.1784 |
| 128.646∠-119.768 | 0.0846∠-68.741 | 0.112∠-75.063 | 0.0295 |
| Inverse Clarke's transformation | | | |
| Input $V_\alpha, V_\beta, V_0$ | Output $V_a, V_b, V_c$ | | |
| | Theoretical | Practical | Error |
| 150.782∠0 | 123.1296∠0 | 122.824∠0 | 0.3056 |
| 152.426∠-90.00 | 124.1475∠-119.738 | 123.635∠-119.743 | 0.5126 |
| 0.063∠-62.865 | 124.0782∠119.7423 | 123.457∠119.827 | 0.8413 |

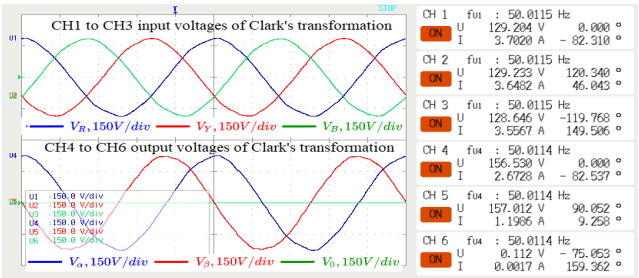


**FIGURE 8.** Responses for modal transformation matrix.

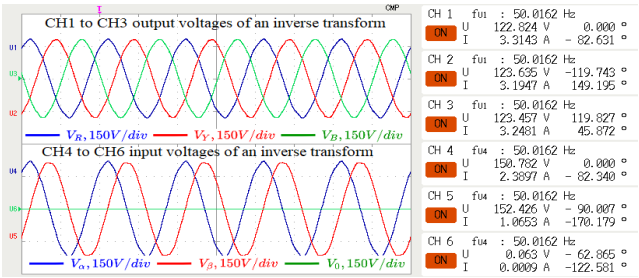


**FIGURE 9.** Responses for inverse modal transformation matrix.

observe that the 3-$\phi$ voltages and modal voltages angular displacements are well maintained. The measured input and output voltages/currents and the expected theoretical calculations are summarized in Table. 5. It can be observed that the magnitude and phase angle errors between the theoretical and the experimental values are very less. These errors can be attributed to the non-ideal transformers. This kind of physical realization of Clarke's and inverse Clarke's transforms is first of its kind effort in the literature to the best of our knowledge.

### B. VALIDATION OF THE SD-LPFD TRANSMISSION LINE

In order to validate the experimental results of the proposed design an attempt is made to simulate the exact experimental setup in EMTP-RV. To achieve this the source impedance of the laboratory distribution grid, where the line is connected

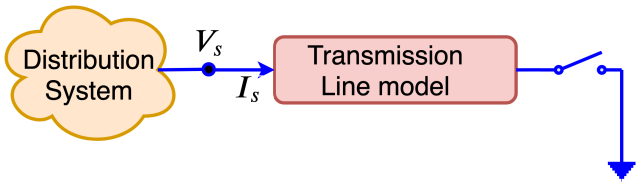


(a) **Test system model**

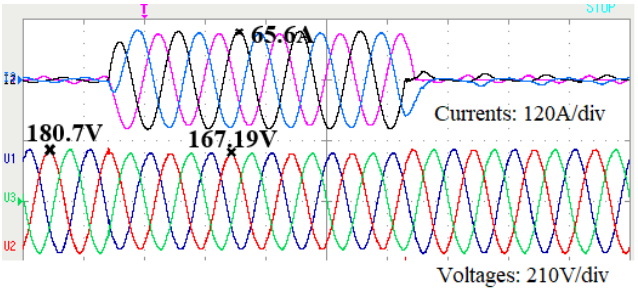


(b) **Sending end currents and voltages**

**FIGURE 10.** Characterization of distribution grid and line impedances.

need to be estimated. The distribution grid and transmission line impedances are obtained by calculating the grid open circuit voltage $V_{Soc}$, short circuit voltage $V_{Ssc}$ and the short circuit current $I_{sc}$ using the test setup shown in Fig.10(a). The measured sending-end short circuit currents and voltages are shown in Fig.10(b). The SD-LPFD line impedance $Z_{tl}$ and the grid impedance $Z_{ds}$ of the distribution grid are calculated as follows from the measurements:

$$Z_{tl} = \frac{V_{Ssc}}{I_{sc}} = \frac{0.9308}{5\angle -48.773} \tag{20}$$

$$= (0.1195 + 0.1435i)pu \tag{21}$$

$$Z_{ds} = \frac{V_{Soc} - V_{Ssc}}{I_{sc}} = \frac{1.006 - 0.9308}{5\angle -48.773} \tag{22}$$

$$= (0.0097 + 0.0116i)pu \tag{23}$$

It can be observed from the values of $Z_{tl}$ and $Z_{ds}$ that the $X/R$ ratio of the modeled line is 1.208. Reproducing low resistance values and accurate inductance values at the low voltage level using copper windings is challenging. In the present

design focus was more on achieving accurate inductance values to maintain smaller sizes. The experimental line is validated by comparing its results with the universal line model (ULM) available in EMTP-RV. The impedance of the ULM in EMTP-RV is also calculated using the above procedure. The *pu* value of the source impedance of the 230 kV ULM in EMTP-RV is maintained to be same as the measured distribution grid [43] for this characterization. The line impedance of ULM in EMTP-RV is obtained as $Z_{tl_{sim}} = (0.0047 + 0.075i)$ *pu*. It can be observed that the X/R ratio of the line is 15.95. The reactance of the experimental line is 0.0685 *pu* higher than the ULM line due to the impedance of the transformers used for transformation. In order to make a fair comparison, ULM in EMTP-RV is simulated with a source impedance of $(0.1245 + 0.0801i)$ *pu* which includes the distribution grid impedance and the additional impedance of the physical line. A constant parameter cascaded $\pi$-model with same number of sections as the experimental line is also simulated in EMTP-RV. Here also the source impedance is modified to take care of the discrepancies in the experimental setup. The following test cases are created on the experimental line as well as in EMTP-RV,

- Voltage transients when an open-ended line is energized.
- Current and voltage transients when a balanced short circuit is applied and removed.
- Current and voltage transients when a $1-\phi$ and a $2-\phi$ unbalanced short circuits are applied and removed.

In the following sections the results of the above test cases are presented. The cascaded $\pi$-model is referred as CP-Line.

### C. SWITCHING TRANSIENTS WHEN AN OPEN ENDED LINE IS ENERGIZED

Open ended experimental line is energized by applying a voltage of 220 V from the lab mains. It can be observed from Fig.8 that the lab mains supply is not a balanced sinusoidal voltage and deviates from 220 V. So, in EMTP-RV simulations of ULM and constant $\pi$-model line, the applied per unit voltages in each phase at 230 kV is matched to the maximum per unit value observed in each phase from the lab mains. The line energization angle is found to be 120.24° of the phase *A* voltage for experimental results. The same switching instant angle is maintained in simulations. Switching transients in the receiving-end voltage are captured using an oscilloscope and they are plotted in *pu* as shown in Fig.11. Simulation results are also provided in *pu*. The peak voltages of *A* and *C* phases are also marked in the figure. It can be seen that the peak voltages observed are more or less same in all the models. The CP-line results show significant wave shape distortion in the transient period. However, smooth sinusoidal wave shape can be observed in the ULM and the experimental line results. This is one unique feature that is expected out of frequency dependent lines. It can be observed that the experimental line transients die down slightly earlier than the other two models. Even though the CP-line tracks the first peak in voltages,

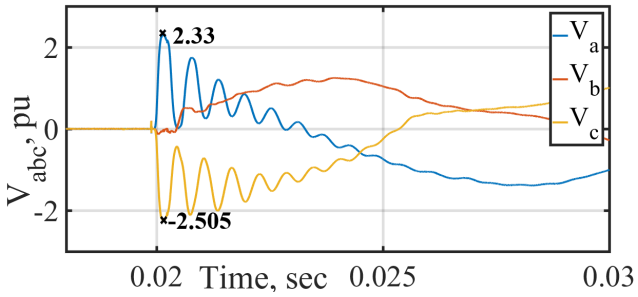


(a) **SD-LPFD line experimental results**

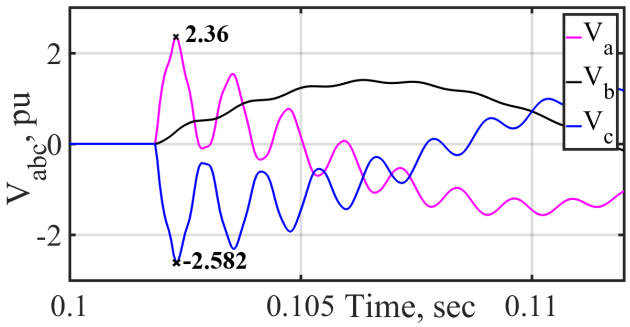


(b) **EMTP-RV simulation of ULM**

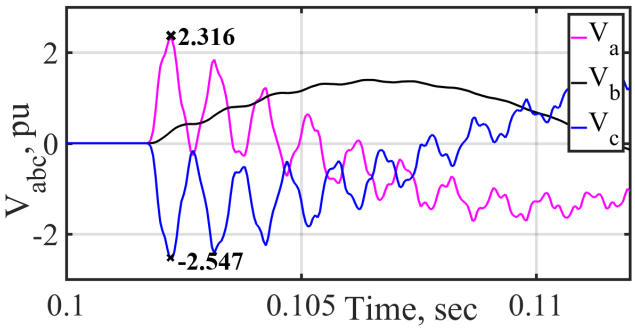


(c) **EMTP-RV simulation of CP line**

**FIGURE 11.** Receiving end voltages for the energization of an open ended line.

subsequent peaks are higher than the ULM. The experimental line peaks closely follow the pattern of ULM. From these energization transients, travel time is calculated as half of the time period of the remote end voltage transients [37]. This traveling time is observed as 0.5 ms for the CP line and 0.3 ms for both the experimental and the ULM.

### D. TRANSIENTS DURING BALANCED SHORT CIRCUITS

The three phases of the energized experimental line are suddenly short circuited at the receiving end. Instant of short circuit found to be around 302.2° of phase *A* voltage. The captured currents at the receiving are plotted in Fig.12. Corresponding simulation results of the ULM and the CP-line are also shown. It can be observed that the peak values of the steady state currents during 3-$\phi$ fault are approximately same for all types of line models. The initial transients quickly die out in the experimental results.

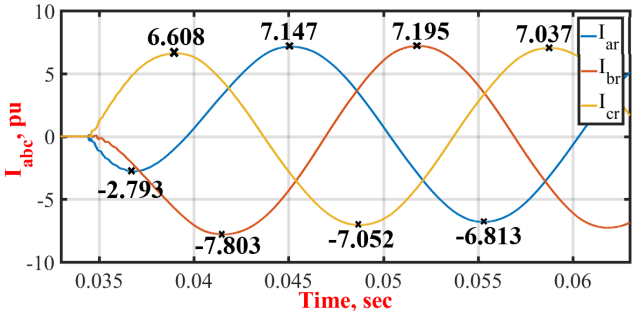


(a) SD-LPFD line experimental Results

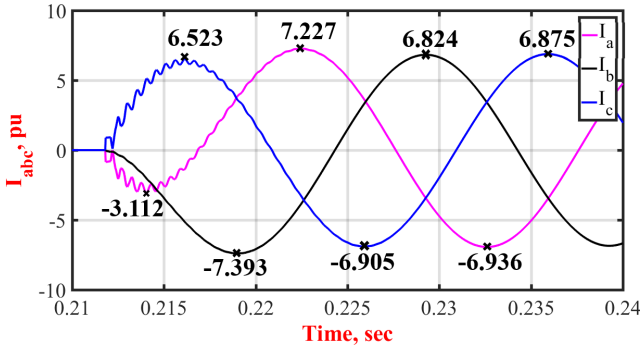


(b) EMTP-RV simulation of ULM

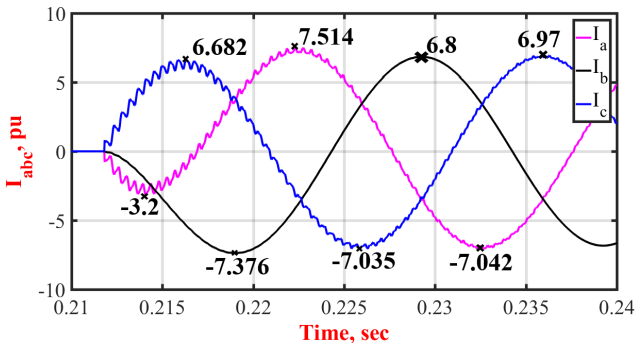


(c) EMTP-RV simulation of CP line

**FIGURE 12.** Currents for 3-$\phi$ short circuit at receiving end.

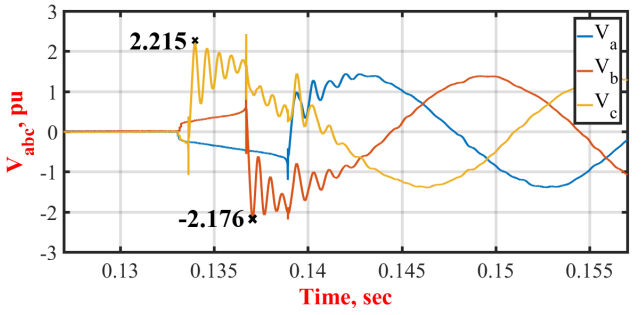


(a) SD-LPFD line experimental results

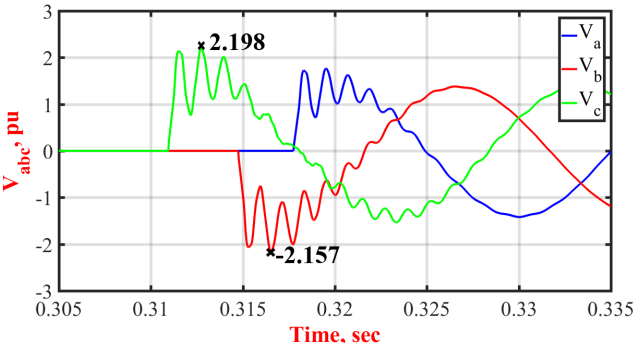


(b) EMTP-RV simulation of ULM

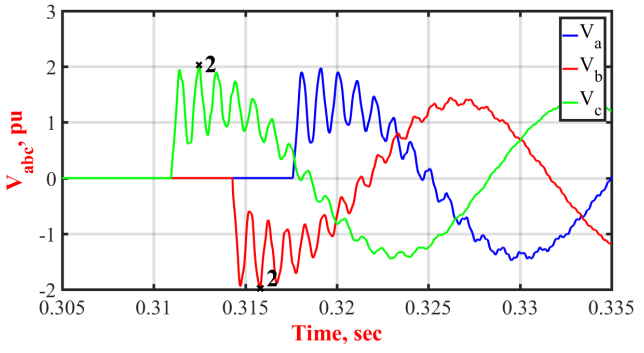


(c) EMTP-RV Simulation of CP line

**FIGURE 13.** Voltages after removal of 3-$\phi$ short circuit.

The short circuit at receiving end is removed after 100 ms and the transients in the receiving voltages are presented in Fig.13. It can be observed that the voltages in all three phases don't rise at the same time and they start increasing at the instant of zero crossings of the corresponding phase currents. The peak voltages and the duration of oscillations of experimental line are close to the ULM. The CP-line results slightly deviate from the ULM. Small residual voltages in the experimental line before the voltages begin to rise are the artifacts of the setup used for short circuit. Both the ULM and the experimental responses follow the same trend i.e. *B* and *C* phases having higher peak than the *A* phase voltage. But, the peak voltages for all the phases are same in the case of CP line. This is another important observation visible in ULM which is properly reproduced in the experimental line.

### *E. TRANSIENTS DURING UNBALANCED SHORT CIRCUITS*

A single phase short circuit of 100 ms duration is created at the receiving end of the experimental line. Instant of short circuit found to be around 120.24° of the phase *A* voltage. The short circuit currents and the voltages after the fault removal at the receiving for the experimental line and the simulation models are shown in Fig.14 and Fig.15 respectively. Voltages during the fault are also captured.

From Fig.14, it can be observed that the 1-$\phi$ fault currents of the experimental line closely follow the ULMresults. However, the CP-line deviations from the ULM are more pronounced. It can be observed that 1-$\phi$ and 3-$\phi$ fault currents are almost equal for the CP line except for the first peak. However, significant difference between the 1-$\phi$ and 3-$\phi$ fault currents can be observed for ULM which is closely mimicked by the experimental line. It can be observed from the ULM

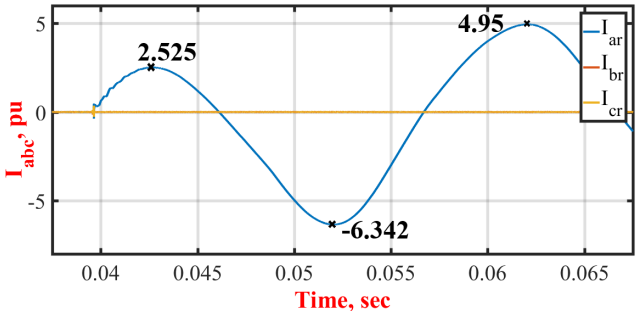


(a) SD-LPFD line experimental results

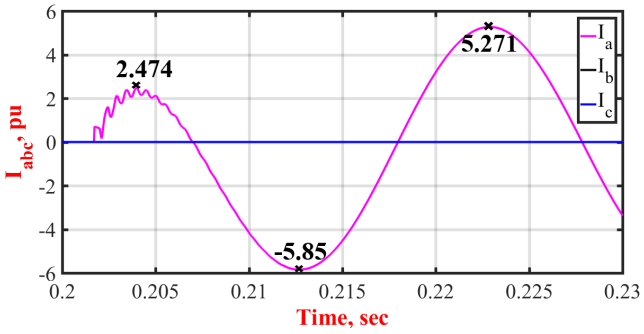


(b) EMTP-RV simulation of ULM

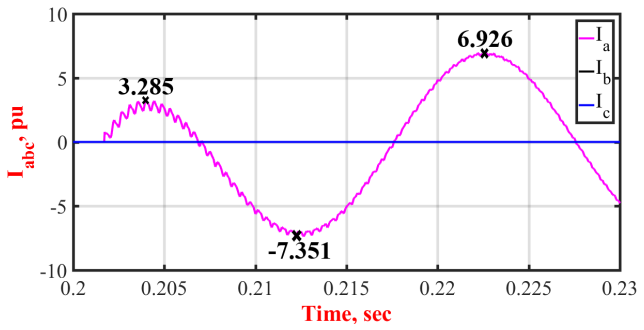


(c) EMTP-RV simulation of CP line

**FIGURE 14.** Currents for 1-$\phi$ short circuit.

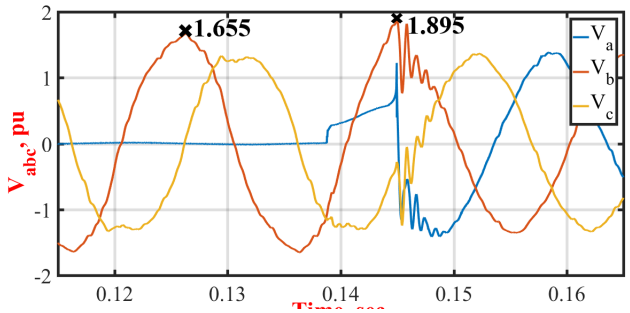


(a) SD-LPFD line experimental results

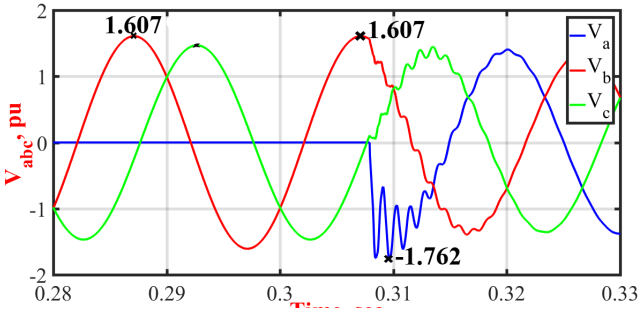


(b) EMTP-RV simulation of ULM

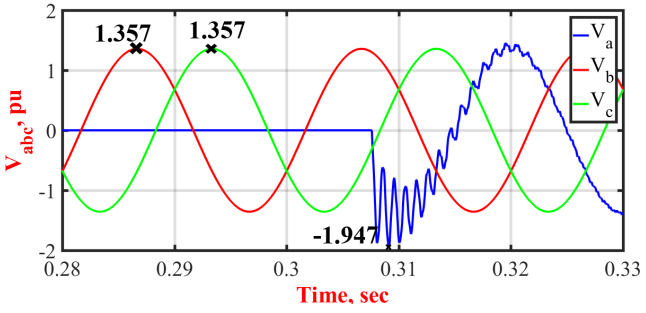


(c) EMTP-RV simulation of CP line

**FIGURE 15.** Voltages after removal of 1-$\phi$ short circuit.

results in Fig.15 that the phase *B* peak voltage is higher than the phase *C* peak voltage during the short circuit, these peaks are approximately remain the same after fault removal. These features are closely mimicked by the experimental line. Slightly higher peak in the phase *B* of the experimental line is observed due to the irregularities in the contactors used in fault creation. However, the voltages of the *B* and *C* phases in the CP-line during the short circuit are equal and remain the same after fault removal. These peaks are smaller than the ULM.

Double line to ground short circuit (A-B-ground) with 100 ms duration is created on the receiving end of the experimental line. Instant angle is found to be at 206.8° of the phase *A* voltage. The corresponding short circuit currents and the voltages after the fault removal at the receiving are shown in Fig.16 and Fig.17 respectively. During the fault, the ULM fault currents show noticeable unbalance which are closely matching with the experimental line. The CP-line fault currents, although show slight unbalance, they are not as much noticeable as ULM. These fault currents in both the ULM and the experimental line are lesser than the 3-$\phi$ fault currents but the CP-line fault currents are closer to the 3-$\phi$ fault currents. From Fig.17, it is evident that the healthy phase voltage during fault is higher than the post-fault value value in both the experimental and the ULM. But, the healthy phase voltage remains approximately same as the post-fault value in case of the CP line. The transient peak voltages after the fault removal are more or less same in all the models. Small oscillations can be observed in the healthy phase voltage in ULM after the fault removal and they are properly captured in the experimental line. However the CP-line shows no oscillations.

Several balanced and unbalanced fault cases are tested by varying the fault duration and the incidence angle. In all these cases same observations are made. From the above balanced

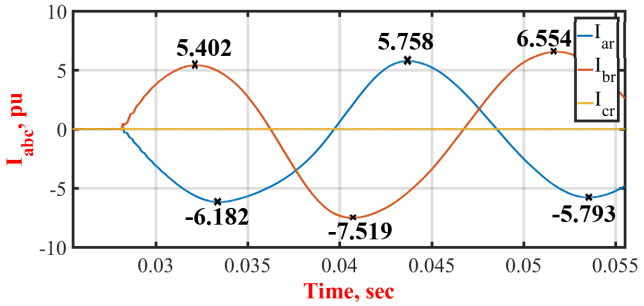


(a) SD-LPFD line experimental results

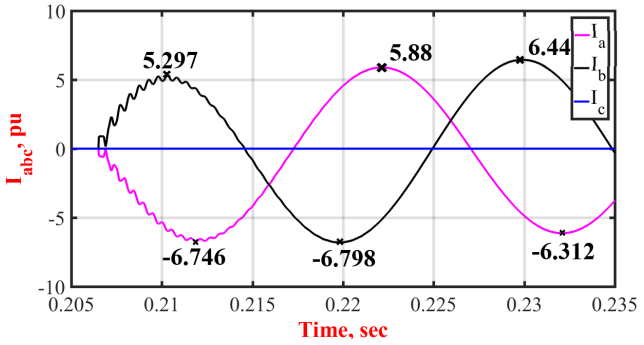


(b) EMTP-RV simulation of ULM

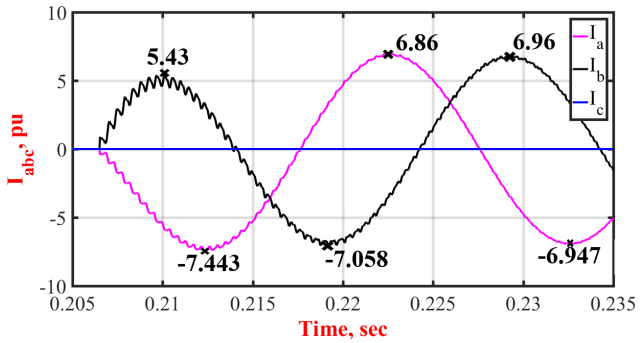


(c) EMTP-RV simulation of CP line

**FIGURE 16.** Currents for 2-$\phi$ short circuit.

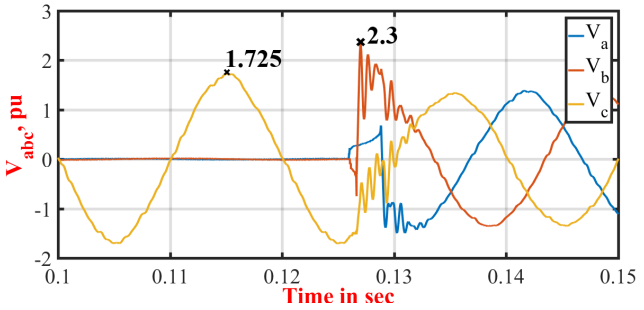


(a) SD-LPFD line experimental results

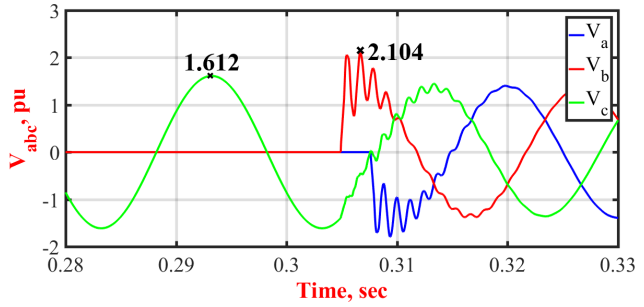


(b) EMTP-RV simulation of ULM

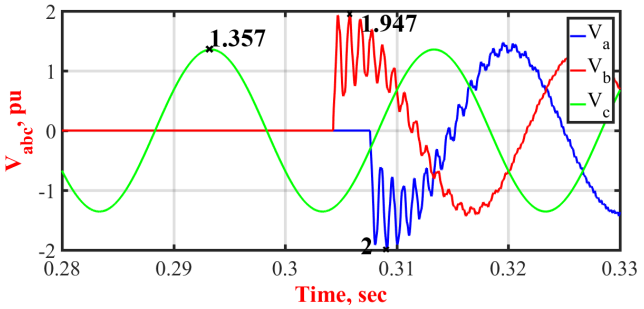


(c) EMTP-RV simulation of CP line

**FIGURE 17.** Voltages after removal of 2-$\phi$ short circuit.

and unbalanced fault scenarios, the imbalances in the voltages and currents visible in the ULM which could not be observed in the CP-line are faithfully reproduced by the experimental line. Although the frequency responses of the LPFD line are matched well with the actual frequency responses, much faster decaying transients and some residual voltages at the fault instant can be observed in the time domain responses of the experimental LPFD line. These deviations can be attributed to the higher internal resistance of the inductors which result in higher $X/R$ ratio and the artifacts of the mechanical contactors used for creating the short circuit faults in the experimental setup. More efficient transformer and inductor designs can be used to improve the performance of the proposed model. Through this work, possibility of developing experimental scaled-down frequency dependent transmission line models is satisfactorily verified for the first time in the literature to the best of our knowledge.

## V. CONCLUSION

Development of a scaled-down lumped parameter frequency dependent transmission line model is proposed in this paper. A 50 km, 220 V scaled-down model of a 230 kV transmission line is developed which represents one of the transmission lines of WECC 3-machine 9 bus system in per unit sense. Detailed calculations are presented for the 1-$\phi$ transformer ratings used in implementing the Clarke's and inverse Clarke's transformations. Amorphous core inductors are used to reproduce the switching transients over a wide range of frequency and their design details are presented in this paper. The developed experimental line is found to closely reproduce the characteristics of frequency dependent line model (ULM) available in EMTP-RV during line energization, balanced and unbalanced scenarios which couldn't be reproduced with a constant parameter $\pi$-model. Especially in case of unbalanced faults, magnitudes of CP line fault currents are largely deviated from the ULM when compared to

the developed experimental line. So, the proposed line model is the best alternative for the CP line which is extensively used in proof of concepts in power systems.

## ACKNOWLEDGMENT

The authors would like to thank M-Core Technologies Private Limited, Bengaluru, India, for their partial support towards the article processing charges.

## REFERENCES

[1] X. Lin and P. Zadkhast, "Study of transmission/distribution network with large number of power electronic devices using hybrid simulation," *IEEE Power Energy Mag.*, vol. 18, no. 2, pp. 106–116, Mar. 2020.

[2] M. Foley, Y. Chen, and A. Bose, "A real time power system simulation laboratory environment," *IEEE Trans. Power Syst.*, vol. 5, no. 4, pp. 1400–1406, Nov. 1990.

[3] I. Etxeberria-Otadui, V. Manzo, S. Bacha, and F. Baltes, "Generalized average modelling of FACTS for real time simulation in ARENE," in *Proc. IEEE 28th Annu. Conf. Ind. Electron. Soc. (IECON)*, vol. 2, Nov. 2002, pp. 864–869.

[4] R. Krebs and O. Ruhle, "NETOMAC real-time simulator—A new generation of standard test modules for enhanced relay testing," in *Proc. 8th IEE Int. Conf. Develop. Power Syst. Protection*, vol. 2, Apr. 2004, pp. 669–674.

[5] L.-F. Pak, M. O. Faruque, X. Nie, and V. Dinavahi, "A versatile cluster-based real-time digital simulator for power engineering research," *IEEE Trans. Power Syst.*, vol. 21, no. 2, pp. 455–465, May 2006.

[6] dSPACE GmbH, Paderborn, Germany. (2014). *dSPACE Product Manual*. [Online]. Available: http://www.dspace.com

[7] R. M. Monaro, J. C. M. Vieira, D. V. Coury, and O. P. Malik, "A novel method based on fuzzy logic and data mining for synchronous generator digital protection," *IEEE Trans. Power Del.*, vol. 30, no. 3, pp. 1487–1495, Jun. 2015.

[8] S. P. Panda, K. A. Salunkhe, and A. M. Kulkarni, "Experimental validation of waveform relaxation technique for power system controller testing," *Sadhana-Acad. Eng. Sci.*, vol. 40, no. 1, pp. 89–106, Feb. 2015.

[9] B. G. Fernandes, A. M. Kulkarni, S. V. Kulkarni, and S. A. Khaparde, "Power engineering laboratories at IIT bombay," in *Proc. IEEE PES Gen. Meeting*, Jul. 2008, pp. 1–5.

[10] G. Wilson, R. Challen, and D. Bosack, "Transmission line models for switching studies: Design criteria I. Effects of non transposition and frequency," *IEEE Trans. Power App. Syst.*, vol. PAS-93, no. 1, pp. 383–388, Jan. 1974.

[11] G. Wilson and K. Schmidt, "Transmission line models for switching studies: Design criteria II. Selection of section length, model design and tests," *IEEE Trans. Power App. Syst.*, vol. PAS-93, no. 1, pp. 389–395, Jan. 1974.

[12] T. Dhaene and D. de Zutter, "Selection of lumped element models for coupled lossy transmission lines," *IEEE Trans. Comput.-Aided Design Integr. Circuits Syst.*, vol. 11, no. 7, pp. 805–815, Jul. 1992.

[13] X.-P. Zhang and H. Chen, "Analysis and selection of transmission line models used in power system transient simulations," *Int. J. Electr. Power Energy Syst.*, vol. 17, no. 4, pp. 239–246, Aug. 1995.

[14] C. J. Truax, J. D. Brown, and W. Neugebauer, "TNA study of reclosing transients on a 765 kV shunt compensated transmission line," *IEEE Trans. Power App. Syst.*, vol. PAS-97, no. 4, pp. 1447–1457, Jul. 1978.

[15] A. A. Hameed, A. Gupta, A. S. Kiranraj, A. G. Devendran, and P. Raja, "Modeling and implementation of impedance based fault locator for medium transmission line," in *Proc. Int. Conf. Condition Assessment Techn. Electr. Syst. (CATCON)*, Dec. 2015, pp. 111–115.

[16] M. Murali, V. N. Pande, and N. Gopalakrishnan, "Design, analysis, fabrication, and testing of laboratory model of transmission line," *Electr. Power Compon. Syst.*, vol. 43, no. 11, pp. 1215–1224, Jul. 2015.

[17] S. N. Ananthan, R. Padmanabhan, R. Meyur, B. Mallikarjuna, M. J. B. Reddy, and D. K. Mohanta, "Real-time fault analysis of transmission lines using wavelet multi-resolution analysis based frequency-domain approach," *IET Sci., Meas. Technol.*, vol. 10, no. 7, pp. 693–703, Oct. 2016.

[18] A. Dwivedi, B. Mallikarjuna, D. Pal, M. J. B. Reddy, and D. K. Mohanta, "A real-time synchrophasor-based zone-3 supervision of distance relays under load encroachment condition," *IEEE Syst. J.*, vol. 13, no. 4, pp. 4227–4235, Dec. 2019.

[19] T. Ono and H. Matsubara, "Number of sections necessary for transmission line model used for transient network analyzer," *Electr. Eng. Jpn.*, vol. 95, no. 5, pp. 415–422, Sep. 1975.

[20] A. P. S. Meliopoulos, G. J. Cokkinides, S. Mohagheghi, Q. B. Dam, R. H. Alaileh, and G. K. Stefopoulos, "A laboratory setup of a power system scaled model for testing and validation of EMS applications," in *Proc. IEEE Bucharest PowerTech*, Jun. 2009, pp. 1–8.

[21] B. Liu, S. Zheng, Y. Ma, F. Wang, and L. M. Tolbert, "Control and implementation of converter based AC transmission line emulation," in *Proc. IEEE Appl. Power Electron. Conf. Exposit. (APEC)*, Mar. 2015, pp. 1807–1814.

[22] S. Zhang, B. Liu, S. Zheng, Y. Ma, F. Wang, and L. M. Tolbert, "Development of a converter-based transmission line emulator with three-phase short-circuit fault emulation capability," *IEEE Trans. Power Electron.*, vol. 33, no. 12, pp. 10215–10228, Dec. 2018.

[23] S. Dutta, S. Mazumdar, and K. Basu, "Power electronic converter based flexible transmission line emulation," *IEEE Trans. Ind. Electron.*, vol. 67, no. 8, pp. 6195–6205, Aug. 2020.

[24] A. Gole, "Modeling guidelines for switching transients report prepared by the switching transients," in *Proc. IEEE Modeling Anal. Syst. Transients Work. Group*, 1998.

[25] A. Budner, "Introduction of frequency-dependent line parameters into an electromagnetic transients program," *IEEE Trans. Power App. Syst.*, vol. PAS-89, no. 1, pp. 88–97, Jan. 1970.

[26] W. Meyer and H. Dommel, "Numerical modelling of frequency-dependent transmission-line parameters in an electromagnetic transients program," *IEEE Trans. Power App. Syst.*, vol. PAS-93, no. 5, pp. 1401–1409, Sep. 1974.

[27] A. Semlyen, "Contributions to the theory of calculation of electromagnetic transients on transmission lines with frequency dependent parameters," *IEEE Trans. Power App. Syst.*, vol. PAS-100, no. 2, pp. 848–856, Feb. 1981.

[28] A. Semlyen and R. Brierley, "Stability analysis and stabilizing procedure for a frequency dependent tansmission line model," *IEEE Trans. Power App. Syst.*, vol. PAS-103, no. 12, pp. 3578–3586, Dec. 1984.

[29] J. R. Marti, "Accurate modeling of frequency-dependent transmission lines in electromagnetic transient simulations," *IEEE Power Eng. Rev.*, vol. PER-2, no. 1, pp. 29–30, Jan. 1982.

[30] A. Morched, B. Gustavsen, and M. Tartibi, "A universal model for accurate calculation of electromagnetic transients on overhead lines and underground cables," *IEEE Trans. Power Del.*, vol. 14, no. 3, pp. 1032–1038, Jul. 1999.

[31] B. Gustavsen, "Frequency-dependent transmission line modeling utilizing transposed conditions," *IEEE Trans. Power Del.*, vol. 17, no. 3, pp. 834–839, Jul. 2002.

[32] J. Schoene and T. E. McDermott, "Modeling large-scale power systems with frequency-dependent transmission line models," in *Proc. IEEE/PES Transmiss. Distrib. Conf. Expo.*, Apr. 2008, pp. 1–7.

[33] T. Noda, "Application of frequency-partitioning fitting to the phase-domain frequency-dependent modeling of underground cables," *IEEE Trans. Power Del.*, vol. 31, no. 4, pp. 1776–1777, Aug. 2016.

[34] A. Takeshige, Y. Ito, K. Takano, K. Katayama, T. Yoshida, M. Fujishima, and S. Amakawa, "Causal transmission line model incorporating frequency-dependent linear resistors," in *Proc. IEEE 21st Workshop Signal Power Integrity (SPI)*, May 2017, pp. 1–4.

[35] H. Ye and K. Strunz, "Multi-scale and frequency-dependent modeling of electric power transmission lines," *IEEE Trans. Power Del.*, vol. 33, no. 1, pp. 32–41, Feb. 2018.

[36] E. C. M. Costa, S. Kurokawa, J. Pissolato, and A. J. Prado, "Efficient procedure to evaluate electromagnetic transients on three-phase transmission lines," *IET Gener., Transmiss. Distrib.*, vol. 4, no. 9, pp. 1069–1081, Sep. 2010.

[37] G. Gurrala, P. Mukherjee, and K. K. Challa, "Reduced order model of a lumped parameter frequency dependent transmission line," in *Proc. 9th Int. Conf. Power Energy Syst. (ICPES)*, Dec. 2019, pp. 1–6.

[38] M. C. Tavares, J. Pissolato, and C. M. Portela, "New mode domain multiphase transmission line model-clarke transformation evaluation," in *Proc. Int. Conf. Power Syst. Technol. (POWERCON)*, vol. 2, 1998, pp. 860–864.

[39] M. C. Tavares, J. Pissolato, and C. M. Portela, "Mode domain multiphase transmission line model-use in transient studies," *IEEE Trans. Power Del.*, vol. 14, no. 4, pp. 1533–1544, Oct. 1999.

[40] M. C. Tavares, J. Pissolato, and C. M. Portela, "Quasi-modes three-phase transmission line model—Transformation matrix equations," *Int. J. Electr. Power Energy Syst.*, vol. 23, no. 4, pp. 323–331, May 2001.

[41] M. Tavares, J. Pissolato, and C. Portela, "Quasi-modes three-phase transmission line model—Comparison with existing frequency dependent models," *Electr. Power Syst. Res.*, vol. 56, no. 2, pp. 167–175, 2000.
[42] A. J. Prado, J. P. Filho, M. C. Tavares, and C. M. Portela, "Representing a double three-phase transmission line in a transient study—A new approach," in *Proc. IEEE Power Eng. Soc. Winter Meeting. Conf.*, vol. 2, Jan./Feb. 2001, pp. 884–889.
[43] K. K. Challa and G. Gurrala, "Scaled down model of WECC 3-machine 9-bus system with frequency-dependent lines," in *Proc. 9th Int. Conf. Power Energy Syst. (ICPES)*, Dec. 2019, pp. 1–6.
[44] C. M. Portela and M. C. Tavares, "Six-phase transmission line-propagation characteristics and new three-phase representation," *IEEE Trans. Power Del.*, vol. 8, no. 3, pp. 1470–1483, Jul. 1993.
[45] M. C. Tavares, J. Pissolato, and C. M. Portela, "Mode domain multiphase transmission line model-use in transient studies," *IEEE Trans. Power Del.*, vol. 14, no. 4, pp. 1533–1544, Oct. 1999.
[46] J. C. C. Campos, J. P. Filho, A. J. Prado, and S. Kurokawa, "Single real transformation matrices applied to double three-phase transmission lines," *Electr. Power Syst. Res.*, vol. 78, no. 10, pp. 1719–1725, Oct. 2008.
[47] *Project 230-kV Power Transmission Line Lethebridge, Alberta-Great Falls, Montana*, Appl. Presidential Permit Montata Alberta Tie Ltd., 2005.
[48] K. K. Challa, G. Gurrala, and P. Mukherjee, "An algorithm for fitting passive equivalent circuits for lumped parameter frequency dependent transmission line models," *IET Gener., Transmiss. Distrib.*, Mar. 2021.
[49] V. John, B. P. Channegowda, N. Mukherjee, A. Krishnan, and A. Karant, "Optimization of higher order filters for grid connected high frequency power converters," Indian Inst. Sci., Bengaluru, India, Project Rep., 2009.
[50] T. Bulletin. Power lite inductor cores: Magnatization curves. Hitachi Met. Amer. Ltd. [Online]. Available: https://www.hitachimetals.com

**KIRAN KUMAR CHALLA** (Member, IEEE) received the B.Tech. degree in electrical and electronics engineering from the Gudlavalleru Engineering College, Gudlavalleru, in 2008, and the M.E. degree in electrical engineering from the Indian Institute of Science, Bengaluru, India, in 2010, where he is currently pursuing the Ph.D. degree with the Department of Electrical Engineering. He was an Assistant Professor with the CVR College of Engineering, Hyderabad, India, from 2010 to 2012, and the ACE Engineering College, Hyderabad, from 2012 to 2014. His research interests include power system stability, application of estimation theory, and control of power systems.

**GURUNATH GURRALA** (Senior Member, IEEE) received the B.Tech. degree from the Sri Venkateswara Hindu College of Engineering, Machilipatnam, India, in 2001, the M.Tech. degree from the JNTU College of Engineering, Anantapur, India, in 2003, and the Ph.D. degree from the Indian Institute of Science, Bengaluru, India, in 2010.

He was an Assistant Professor with the SSN College of Engineering, Ongole, India, from 2001 to 2002, and the Anil Neerukonda Institute of Technology and Sciences (ANITS), Visakhapatnam, India, from 2003 to 2005. He was a Research Engineer with the GE Global Research, Bengaluru, from 2010 to 2012. He was a Postdoctoral Fellow with Texas A&M University, USA, from 2012 to 2013, and the Oak Ridge National Laboratory, USA, from 2014 to 2015. He is currently an Assistant Professor with the Department of Electrical Engineering, Indian Institute of Science. His research interests include smart grids, power system stability, grid integration of renewables, microgrid control, high-performance computing applications to power systems, nonlinear, and adaptive control of power systems. He is also a Senior Member of the INAE Young Associate. He received the SERB-STAR Award 2020, the IEEE PES Outstanding Engineer Award 2018, and the INAE Young Engineer Award 2015. His articles received the Best Paper Award from ICPS 2019, IEEE General meeting 2015, best poster awards in IEEE industrial society annual meeting 2015, and EEE PES T&D Conference and Exposition 2016. Four of his master students received POSOCO power system awards.